Material Investigations and Optical Properties of Phthalocyanine Nanoparticles

Christian Nitschke, Sean M. O'Flaherty, Michael Kröll, and Werner J. Blau*

Department of Physics, Trinity College Dublin, Dublin 2, Republic of Ireland

Received: June 6, 2003; In Final Form: November 12, 2003

We report a method for the fabrication of phthalocyanine particles with dimensions in the nanoscale regime. Phthalocyanines are of particular interest as reversed saturable absorption-based optical limiters. By fabricating phthalocyanine particles of nanometer sizes, we found intermolecular effects to strongly influence the linear and nonlinear optical properties. Linear optical studies, including absorption and emission spectroscopy, were used to investigate the interactions between the molecules inside the particles. The Z-scan technique was employed to examine the optical limiting effects in phthalocyanine nanoparticles compared to solutions of the corresponding molecules. Transmission electron microscopy (TEM) and atomic force microscopy (AFM) studies were performed to further investigate the particle structure. Furthermore, X-ray diffraction measurements were made to probe the molecular alignment in the nanoparticle.

1. Introduction

With the development of the laser and other high-intensity visible-light sources it has been recognized that optical instruments, especially the human eye, can easily be damaged by unwanted irradiation. Therefore, the need for optical limiters has generated much interest in the development of new nonlinear optical materials and devices[1] for such applications. In general, an optimal optical limiting material has a high dissipative extinction nonlinearity, an inherently fast response time, a large dynamic range, and a broadband spectral response. Therefore, it will strongly attenuate intense, highly dangerous light, which could damage the device, but will exhibit high transmission for low intensity ambient light.

A variety of materials such as semiconductors,[2,3] fullerenes,[4−6] carbon nanotubes,[7−12] polymer−carbon nanotube composites,[13,14] and metal clusters[15−18] have been studied for this application. In recent years, much interest has been focused on optical limiters fabricated from organic materials, as opposed to inorganic materials, due to their low production costs and ease of processing.[19−22] Phthalocyanines (Pc) have emerged as one of the most promising materials from the large number of organic optical limiting materials that have been studied. The most evident advantages are the large nonlinear optical coefficients and their ultrafast response time. Additionally, the molecular structure is highly versatile and can be easily modified with chemical modifications on the phthalocyanine ring.[23] Also, many different metallic and nonmetallic cations can be accommodated in the ring cavity. It is also possible to alter the axial substituent at the central metal atom and the peripheral substituents of the macrocycle.[24]

Optical limiting by phthalocyanines was first reported by Coulter et al.[25] He demonstrated the optical limiting effect in a chloroaluminum phthalocyanine (PcAlCl). Subsequently, a large number of other phthalocyanine compounds has been investigated, for example, PcInCl,[26] tBu$_4$PcIn(p-TMP),[26] and PbPc-(β−CP)$_4$.[27] Perry et al.[28] prepared a practical optical limiting device using a tetra-substituted chloroindium phthalocyanine in an inhomogeneous distribution along the beam path. This device was able to attenuate nanosecond irradiation by factors of up to 540.

There is still interest in modifying and optimizing phthalocyanine structure properties for different optical limiting purposes.[29] However, in recent years a different area of research in optical limiting has become more important. In this method, fabrication of systems that initially function without detailed study of form has dominated research efforts. Subsequently, the form of a functioning system is explored. The investigation of cocrystallization of merocyanine dyes showed different nonlinear optical behavior depending on the crystal structure.[30] Desiraju[31] has reviewed most of this type of work, which has been dubbed "crystal engineering". One of the biggest issues with this method is to control the alignment and structure of these crystals or highly ordered systems.[32,33] An increase in nonlinearity and optical limiting for polymeric, microcrystalline particles and thin films compared to their molecules has also previously been reported.[34−35]

In this paper, a detailed study of phthalocyanine nanoparticles, fabricated using the "microwave method", which has been found to be a suitable method for controlled fabrication of organic nanoparticles,[33] is described. The change in the linear and nonlinear optical properties of these nanoparticles, compared to their molecules in solution, is addressed, and furthermore, a series of microscopic and spectroscopic methods has been used to investigate the nanoparticle structure.

2. Experimental Section

2.1. Particle Preparation. The phthalocyanines used in this study were purchased from Aldrich (zinc 2,9,16,23-tetra-*tert*-butyl-29H,31H -phthalocyanine (tBu$_4$PcZn), zinc 2,9,16,23-tetrakis-(phenylthio)-29H,31H-phthalocyanine ((PhS)$_4$PcZn), copper 2,9,16,23-tetra-*tert*-butyl-29H,31H-phthalocyanine (tBu$_4$PcCu), and 2,9,16,23-tetrakis-(phenylthio)-29H,31H-phthalocyanine ((PhS)$_4$PcH$_2$)); product codes (PhS)$_4$PcZn 41,823-4, tBu4PcZn 43,099-4, tBu$_4$PcCu 42,316-5, and (PhS)$_4$PcH$_2$) 41,818-8). Phthalocyanines dissolved in freshly distilled acetone solutions were prepared at concentrations on the order of 1 g/L (actual values quoted in Table 1) and subjected to low-power sonication

* Corresponding author. Tel: +353 1 6081708. Fax: +353 1 6711759. E-mail: wblau@tcd.ie.

10.1021/jp035604e CCC: $27.50
Published on Web 12/24/2003

TABLE 1: Concentration of the Phthalocyanine−Acetone Solutions, Volumes of Phthalocyanine−Acetone Solution Injected into 20 mL of Water, and Resulting Nanoparticle Dispersion and Molecular Solution Concentration

Pc compound	concentration [g/L]	injected volume of acetone solution [μL]	concentration of nanoparticle dispersions [g/L]
tBu$_4$PcCu	1.0	200	0.01
(PhS)$_4$PcH$_2$	1.2	300	0.012
(PhS)$_4$PcZn	0.7	200	0.007
tBu$_4$PcZn	1.0	200	0.01

(60 W) to ensure complete and uniform dispersal. The dye contents (purity level) given by Aldrich were included in the concentration calculations, where after sonication the samples were left to stand undisturbed for a period of time to allow the principally inorganic impurities settle. Furthermore, the samples were stored in a closed volumetric cylinder in the dark to avoid any kind of unwanted photochemical reaction initiated by sunlight or air. These molecular solutions were considered to be homogeneous, and the possible aggregation in these starting solutions was considered to be negligible.

Nanoparticles were produced by a combination of the reprecipitation method and microwave irradiation,[33] termed the "microwave method". Recently, we have used this combination to produce phthalocyanine nanoparticles from zinc-centered phthalocyanines.[36] The reprecipitation method is known in organic and inorganic chemistry as a good method to form nanoparticles.[35,37−39] Additionally, the treatment of metals and semiconductors with microwave irradiation to form monodispersed small particles is also well-known.[40−42] Thus, the nanoparticle preparation procedure for these phthalocyanine compounds was as follows: 200 μL of the phthalocyanine−acetone solution (carefully syringed from the top of the sample vial to minimize the potential presence of inorganic impurities) was injected into 20 mL of vigorously stirred deionized water at room temperature using a microsyringe. After injection, the aqueous nanoparticle dispersion was irradiated immediately using a microwave oven (Sharp Compact R-230A; 2.45 GHz, 800 W) at 560 W for 30 s. The treatment with microwaves is considered to be a homogeneous irradiation of the entire droplet liquid dispersion system formed after reprecipitation. Experimentally, this implies that after injection of the organic solvent solution (phthalocyanine dissolved in acetone in this case) into water, microwaves are employed to heat the dispersion and hence force the organic solvent to evaporate rapidly. The rapid evaporation aims to try to prevent aggregation between droplets. The compound, which was dissolved in the droplet before evaporation, will then form regularly shaped particles of nanometer dimensions. Thus, the final nanoparticle dispersions were at mass concentrations on the order of 0.01 g/L (actual values quoted in Table 1), and to allow the execution of comparable experiments, solutions of the compounds were prepared at the same mass concentrations in DMF. It was noticed that after 24−36 h the dispersions exhibited clustering effects due to collisions between the nanoparticles undergoing thermal diffusion, and thus, all experiments were performed with nanoparticles that were freshly fabricated.

2.2 Optical Experiments. Absorption spectra were recorded using a Shimadzu UV3100 UV−vis−NIR spectrometer. The nanoparticles were dispersed in water and the molecules dissolved in DMF (Aldrich; analyt. grad.) and sonicated, using an ultrasonic bath, for 30 min. While shifts in the spectra due to solvatochromic effect are possibly present, the use of two different solvents was necessary here. The corresponding phthalocyanine nanoparticle and molecular solution pairs were prepared at the same concentration (Table 1).

The phthalocyanine molecule solutions and nanoparticle dispersions, prepared for UV/vis spectroscopy, were also used for emission spectroscopy. The spectra were recorded using a Perkin-Elmer LS55 luminescence spectrometer equipped with a red-sensitive Hamamatsu R298 PMT detector. The measurements were performed using a 1 cm^2 quartz cell.

Optical limiting measurements were performed using the open-aperture Z-scan technique[43] using 6 ns pulses from a Q-switched Nd:Yag laser. The beam was spatially filtered to remove higher-order modes and tightly focused with a 9 cm focal length lens. The laser was operated at its second harmonic, 532 nm, with a pulse repetition rate of 10 Hz. All phthalocyanine molecular solutions and nanoparticle dispersions were prepared in the same way as for the UV/vis studies (Table 1). All measurements were performed in a quartz cell with a 1 cm path length.

2.3. Particle Investigation. TEM was used to investigate the average particle size of the different phthalocyanine nanoparticles. Approximately 2 mL of freshly prepared nanoparticle−water dispersion was immediately dropped onto a copper grid coated with a polymer (Formvar). The water was evaporated under reduced pressure (7−10 mbar) at room temperature (25 °C). The resulting samples were observed using a Hitachi H-7000 transmission electron microscope equipped with a Megaview 2 CCD camera from SIS for electronic picture storage. Due to the low material contrast between the Formvar film and the phthalocyanine nanoparticles most pictures were taken slightly off focus. This produced a white ring around the edge of the particles and hence increased the contrast.

The particle diameters determined by TEM were confirmed by AFM imaging. Furthermore, the height of the nanoparticles could be observed by using this method. The samples were prepared by dropping approximately 3 mL of a freshly prepared nanoparticle/water dispersion onto a 1 cm^2 silicon substrate. The substrate was immediately placed in a vacuum oven, and the water was evaporated under reduced pressure (7−10 mbar) at room temperature (25 °C). The samples were observed using a Digital Instruments Nanoscope IIIa in tapping mode.

A further investigation of the nanoparticle structure was realized using X-ray diffraction. The samples were prepared by dropping approximately 5 mL of freshly prepared nanoparticle dispersion onto a silicon substrate of 2 cm^2 dimension and subsequent evaporation of the solvent in a vacuum oven at room temperature at 7−10 mbar. The resulting particle layer was then covered with grease. The X-ray measurements were performed with a Siemens D500 X-ray diffractometer with a Cu Kα_1 radiation at a wavelength of 1.540 56 Å. In this work, the 2θ geometry is used to characterize the samples.

3. Results and Discussion

3.1. Optical Experiments. In the absorption spectra for the molecular solutions of phthalocyanine in DMF, the typical Q-band and B-band absorptions were located in all cases. Furthermore, the molecule spectra for the tBu$_4$PcZn and the (PhS)$_4$PcZn are in good agreement with those found by Wrobel et al.[44] and agree with that quoted by Aldrich. The spectra for the tBu$_4$PcCu and the (PhS)$_4$PcH$_2$ are in the same region as the corresponding peripheral unsubstituted phthalocyanine molecule[24] (Figure 1) where blue shifts of the Q-bands of 3 nm for tBu$_4$PcCu and 11 nm for (PhS)$_4$PcH$_2$ can be recognized. The splitting of the Q-band for metal-free phthalocyanines due to the reduced D_{2h} symmetry was not located here in the

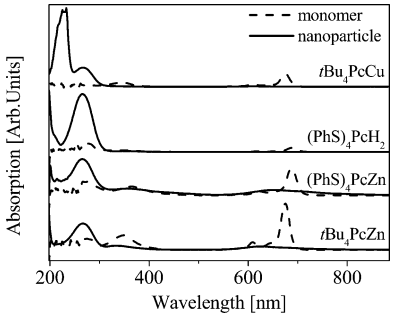

Figure 1. UV/vis spectra. The phthalocyanine molecular solutions are shown in dashed lines and the particle-state phthalocyanine in solid lines. The spectra are absorption-shifted for clarity.

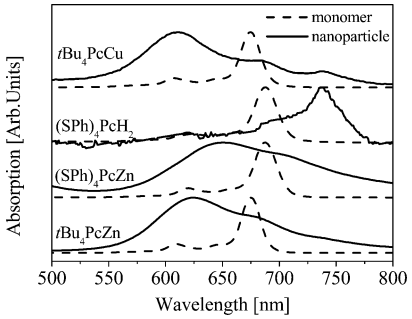

Figure 2. UV/vis spectra of the Q-band region. Nanoparticle states are presented by solid lines and molecular solutions by dashed lines. The spectra are again shifted on the absorption scale for clarity.

TABLE 2: UV/vis Absorption Bands, Areas under the Peaks, and Area Ratios

sample	Q-band [nm]	area Q-band	B-band [nm]	area B-band	area Q/ area B
*t*Bu4PcCu (M)	675 (607)	20.00	252, 342	16.6	1.20
*t*Bu4PcCu (N)	611, 679, 738	2.00	224, 269	143.9	0.014
$(PhS)_4PcH_2$ (M)	688 (622)	4.90	274, 353	21.4	0.230
$(PhS)_4PcH_2$ (N)	738	0.23	198, 285	262.2	0.00088u
$(PhS)_4PcZn$ (M)	687 (619)	45.0	274, 364	39.9	1.13
$(PhS)_4PcZn$ (N)	651, 706, 759	29.8	200, 269, 356	135.2	0.220
*t*Bu4PcZn (M)	675 (609)	64.0	265, 335	41.2	1.56
*t*Bu4PcZn (N)	624, 679, 731	16.4	195, 270, 349	106.7	0.15

$(PhS)_4PcH_2$−DMF solution. Repeated experiments revealed that the Q-band splitting was evident in toluene solutions but not in DMF solutions. This result interesting in its own right was not further considered here. In all cases, the B-band exhibits both an increase and a blue shift for the nanoparticle state. Additionally, an accompanied quenching of the Q-band can be noticed. The locations of and the area under the peaks are presented in Table 2. In the remaining sections of this report, the reference 'M' implies dissolved molecules in solution while 'N' implies the nanoparticles dispersed in deionized water.

Dependent on the phthalocyanine under consideration, the B-band absorption increases by a factor of 2.5 (*t*Bu4PcZn) up to 12.5 ($(PhS)_4PcH_2$) in the nanoparticle state. The peak around 270 nm, which occurs in every nanoparticle spectrum, is most likely due to acetone, which seems to be trapped within the particle. This is caused during the rapid solvent evaporation during the preparation phase where the nanoparticle formation appears to prevent the complete evaporation of the acetone. Endo et al.[45] and Balabana et al.[46] have previously reported this behavior for similar molecules. They showed that the trapped solvent exhibited an influence on the molecular orientation in the aggregated system. Time-dependent studies showed a decrease of this absorption of 30−35% within 2 days. Unfortunately, after 24 h, the nanoparticle dispersions investigated here are no longer suitable for measurements because aggregation of the particles is evident as explained in section 2.1. Nevertheless, the areas of the Q-band exhibited a decrease by a factor of 1.5 for $(PhS)_4PcZn$ to 10 for *t*Bu4PcCu from molecular solution to nanoparticle state. Furthermore, a broadening of the Q-band was observed, as well as a peak shift to red and to blue in the area between 500 and 800 nm. In the interest of clarity, the Q-band absorption areas are explored further in Figure 2 where the molecular and nanoparticle state spectra are normalized to the peak of the Q-band.

For all three phthalocyanines containing a central metal ion, a blue-shifted peak (shorter wavelength) can be seen in the nanoparticle state. Furthermore, the broadened absorption also exhibits components shifted to the red. This broadening is probably due to a mixture of cofacial and edge-to-edge stacked molecules inside the particle.[47,48] Visibly, the intensive green or blue color, characteristic of these phthalocyanine solutions, was found to be much lighter for the nanoparticle samples, directly caused by the Q-band quenching. Shifts in the UV/vis spectra are known to indicate stacking behavior of molecules within an aggregate.[46,49] Czikklely et al.[50] reported a series of different arrangements for dye molecules in aggregates, which could be identified by the position of their blue- and red-shifted absorption bands. In our cases a blue- and a red-shifted band of approximately ±55−65 nm in wavelength, with respect to the molecular peak, in solid state was observed. If one compares this with the data reported by Czikkleley et al.,[50] it seems to imply a slipped cofacial orientation within the aggregated system. Additionally, the molecular peak can still be noted in the Q-band with a slight shift to the red due to the phase shift from solution to solid state. This possibly suggests that this peak represents single molecules, which surround the particle as a shell. The molecules in this shell appear to be in a random order, and for that reason, they will not interact with their neighbor molecules. The nanoparticles of the metal-free phthalocyanine ($(PhS)_4PcH_2$) exhibit an unusual spectrum compared to the other phthalocyanine nanoparticles. A sharp, very weak red-shifted peak was observed, which to a first approximation indicates only edge-to-edge interactions between the molecules. However it is likely that the true effect is far more complex.

The reversibility of the nanoparticle fabrication process was also investigated using linear absorption spectroscopy to determine whether the microwave irradiation had damaged the starting phthalocyanine material. Nanoparticles were prepared as described above. These were verified using linear spectroscopy as outlined and discussed above. The water was then evaporated from these dispersions in Teflon bowls, and the residue phthalocyanine matter was redissolved in DMF. Linear absorption spectroscopy of the final solutions revealed unchanged signature absorption spectra compared to the original phthalocyanine (dissolved in DMF) solutions depicted in Figures 1 and 2. Thus the nanoparticle fabrication method was found to be a completely reversible process.

The molecular fluorescence spectra exhibited a mirroring of the Q-band in the 600−900 nm region (Figure 3). Y. Chen et al.[51] have reported much the same phenomenon for Ga and In phthalocyanine compounds. Additionally, the results obtained for *t*Bu4PcZn and $(PhS)_4PcZn$ are in good agreement with those found by Wrobel et al.[44] All particle measurements were recorded at an excitation wavelength of 200 nm. The excitation wavelength for the molecular solutions was 360 nm because of the strong solvent absorption below that wavelength. It can be seen that the transition from molecular solution to quasi-solid-

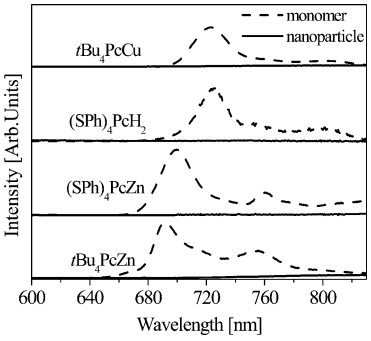

Figure 3. Fluorescence spectra of phthalocyanine. Nanoparticle states are presented by solid lines and molecular solutions by dashed lines. The spectra are shifted on the emission scale for clarity.

TABLE 3: Optical Limiting Results at 532 nm[a]

sample	α_0 [cm^{-1}]	E_{Pulse} [mJ]	β_I [cm W^{-1}]	F_{Sat} [J cm^{-2}]	κ [σ_{ex}/σ_0]
*t*Bu$_4$PcCu (M)	0.082	0.11	$(3.5 \pm 0.7) \times 10^{-10}$	6 ± 1.4	4.4 ± 0.7
*t*Bu$_4$PcCu (P)	0.084	0.24	$(1.5 \pm 0.3) \times 10^{-10}$	100 ± 40	9.6 ± 0.1
(PhS)$_4$PcH$_2$ (M)	0.065	0.27	$(1.0 \pm 0.2) \times 10^{-10}$	9.4 ± 1.8	2.1 ± 0.2
(PhS)$_4$PcH$_2$ (P)	0.071	0.34	$(1.6 \pm 0.3) \times 10^{-11}$	48 ± 45	1.7 ± 0.5
(PhS)$_4$PcZn (M)	0.135	0.20	$(4.0 \pm 0.8) \times 10^{-10}$	20.2 ± 0.2	4.0 ± 1.0
(PhS)$_4$PcZn (P)	0.146	0.30	$(2.1 \pm 0.4) \times 10^{-9}$	18.5 ± 1.4	11.3 ± 0.6
*t*Bu$_4$PcZn (M)	0.100	0.16	$(4.9 \pm 1.0) \times 10^{-10}$	14.2 ± 1.5	5.1 ± 0.4
*t*Bu$_4$PcZn (P)	0.095	0.20	$(1.6 \pm 0.3) \times 10^{-9}$	17.5 ± 3.6	14.6 ± 2.1

[a] The reference (M) implies molecules in solution, while (P) implies the nanoparticles dispersed in deionized water.

state nanoparticle for each phthalocyanine is accompanied in all cases by a complete quenching of the fluorescence. This complete quenching of the bands indicates total nonradiative energy dissipation, which is directly caused by the quasi-solid-state structures. Thus the excitation is dissipated through nonradiative vibrations in the particle rather than photonic emissions in the molecular solutions.

All open aperture Z-scans performed in this study, both from nanoparticle and from molecule samples, exhibited a reduction in the transmission around the focus of the lens. This was typical for an induced positive nonlinear absorption of the incident light, in this case attributed to reverse saturable excited-state absorption. The nonlinear absorption coefficients β_I calculated from these fits[43] are presented in Table 3. It should be noted that the β_I coefficient was not measured over a large intensity range. The nonlinear dissipative response was also investigated using a static approximation to a three-level absorber where normalized absorption was plotted as a function of the incident energy density (F), where $F = E_{Pulse}/(\pi w(z)^2)$ and E_{Pulse} is the energy per laser pulse and $w(z)$ is the beam radius as a function of z in the experiment. These curves, depicted in Figure 4, were fitted with the total absorption coefficient $\alpha_{Total} = \alpha_0(1/(1 + F/F_{Sat}) + \kappa(F/F_{Sat})/(1 + F/F_{Sat}))$, where α_0 is the linear absorption coefficient, κ is the ratio of the ground- to excited-state absorption cross sections, and F_{Sat} is the saturation energy density. κ and F_{Sat} therefore define the magnitude and nature of the nonlinearity and were treated as free parameters in the fitting. It has to be noted at this point that while this model is spectroscopically valid for molecular solutions of phthalocyanine, further experiments are necessary before κ and F_{Sat} can be thought of as "real" parameters for the nanoparticle dispersions. This is discussed further below, and from this point on, it is beneficial to consider the κ and F_{Sat} parameters as coefficients that define the magnitude of the nonlinear response rather than parameters that actually measure molecular properties.

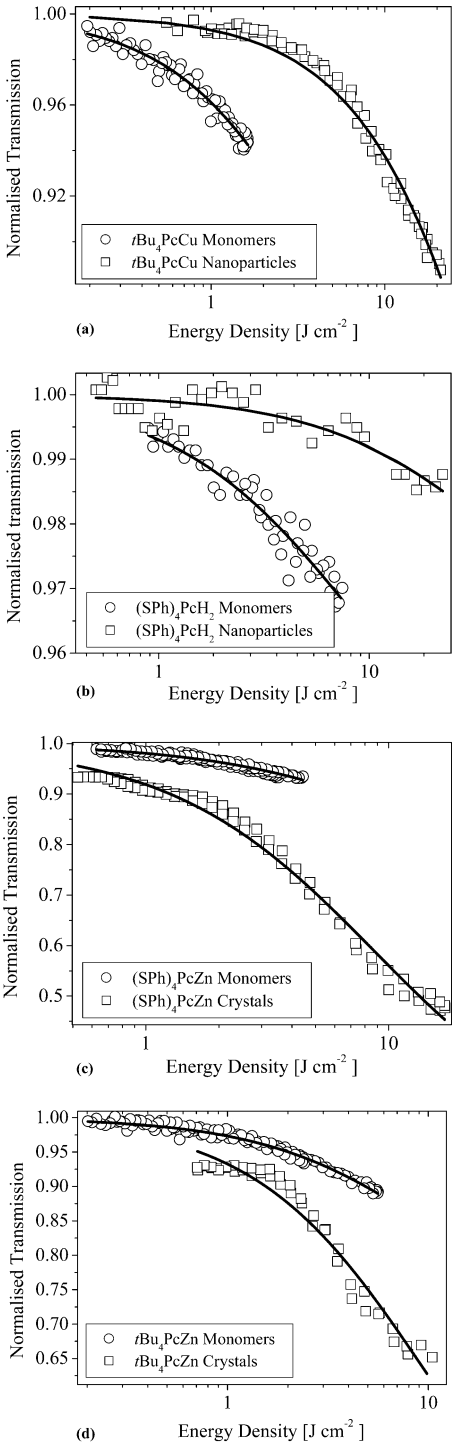

Figure 4. Optical limiting plots for (a) *t*Bu4PcCu, (b) (PhS)$_4$PcH$_2$, (c) (PhS)$_4$PcZn, and (d) *t*Bu$_4$PcZn. The solid lines are theoretical curve fits of the normalized transmission governed by the expression for the nonlinear absorption.

It should be noted that in the case of the Zn phthalocyanines the nonlinear absorption coefficients β_I of the nanoparticles were larger than those for their corresponding monomers. For example, the (PhS)$_4$PcZn monomer exhibited $\beta_I \approx (4.0 \pm 0.8) \times 10^{-10}$ cm W^{-1}, while its associated nanoparticle exhibited a β_I coefficient approximately 5.3 times larger. However, the β_I difference between the monomer and nanoparticle samples was by a factor of approximately 2.3 for the Cu phthalocyanine and 6.3 for the H_2 phthalocyanine with the nanoparticles exhibiting the lesser value.

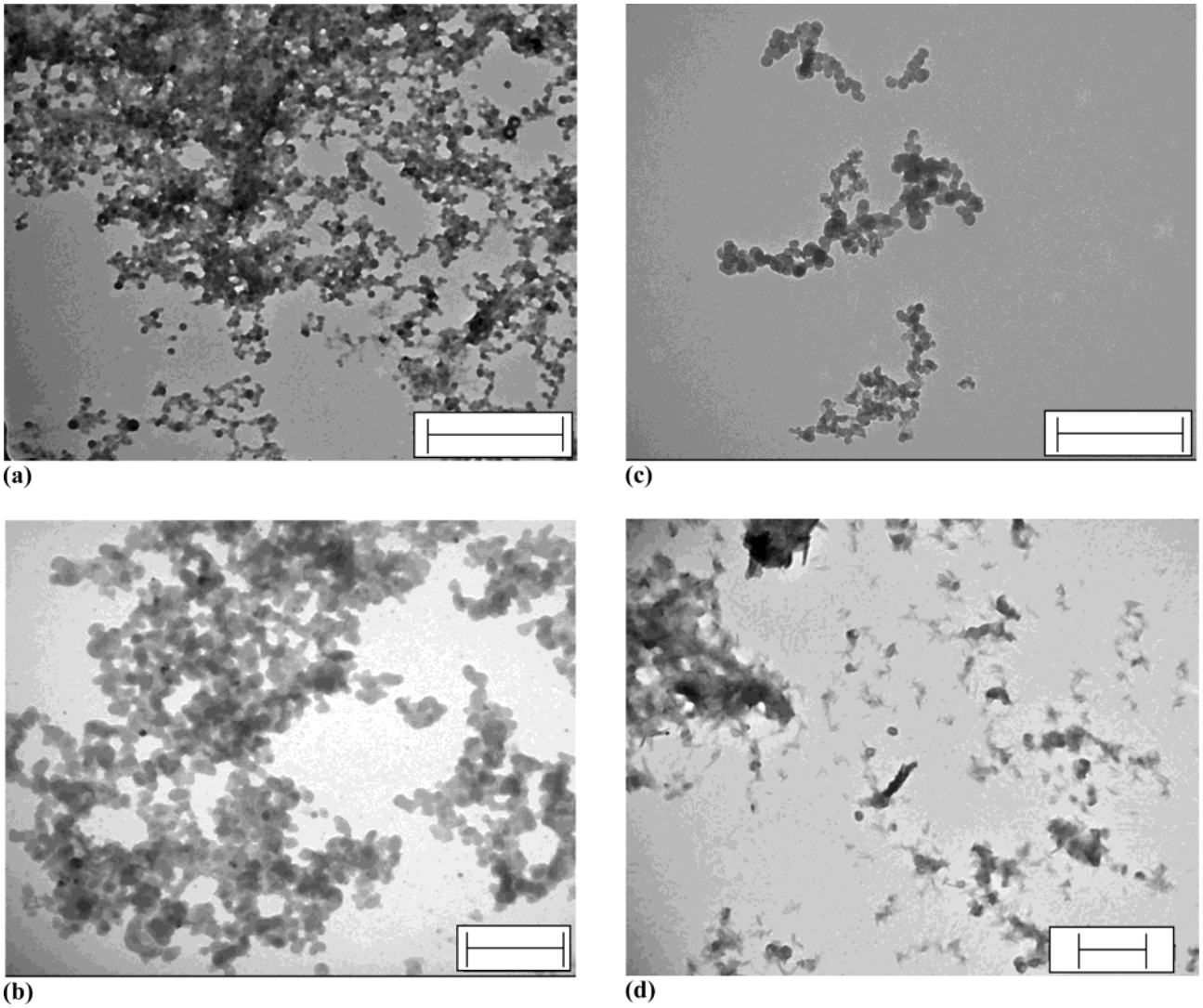

Figure 5. TEM pictures of (a) *t*Bu_4PcCu, (b) $(PhS)_4$PcZn, (c) *t*Bu_4PcZn, and (d) $(PhS)_4PcH_2$. The scale bars in the TEM images represent 0.5 μm.

The linear absorption coefficient α_0 at 532 nm was found to be material-dependent rather than phase-dependent with the $(PhS)_4PcH_2$, $(PhS)_4$PcZn, *t*Bu_4PcZn, and *t*Bu_4PcCu molecules and particles exhibiting similar α_0 coefficients. The linear absorption coefficient exhibited by the $(PhS)_4$PcZn was the highest observed in this series of measurements. This was followed by the *t*Bu_4PcZn and the *t*Bu_4PcCu samples. The sample with the lowest α_0 coefficient was the $(PhS)_4PcH_2$. The saturation density F_{Sat} was slightly reduced from (20.2 $\pm$ 0.2) to (18.5 $\pm$1.4) J cm^{-2} when the $(PhS)_4$PcZn molecules were phase-changed from molecular material to nanoparticles. Conversely, F_{Sat} was increased from (14.2 $\pm$ 1.5) to (17.5 $\pm$ 3.6) J cm^{-2} for the same material composition change for the *t*Bu_4-PcZn samples. The high F_{Sat} values with significant error margins received for *t*Bu_4PcCu and $(PhS)_4PcH_2$ originate from more noisy datasets.

In the past, the ratios of the effective excited- to ground-state absorption coefficients termed κ, where $\kappa = \sigma_{ex}/\sigma_0$ is the ratio of the excited- to ground-state absorption cross sections, have been utilized as an indicator for optical limiting performance. Interestingly the phase shift from molecular to nanoparticle state investigated here has a high impact on the κ coefficient. In the cases of $(PhS)_4$PcZn, *t*Bu_4PcZn, and *t*Bu_4-PcCu, the investigated the κ coefficients were increased. This was by a factor approximately equal to 2.9 for the Zn-containing phthalocyanine and a factor of approximately 2.2 for the Cu phthalocyanine. This is a very significant improvement in the optical limiting response compared to the molecular samples. These results are in good agreement with those found for polymeric compounds.[36] For the $(PhS)_4PcH_2$ no major change for κ between molecule and nanoparticle state could be noticed. The representative optical limiting plots are presented in Figure 4.

The origin of the optical nonlinearity exhibited by the nanoparticle dispersions was not investigated in this study. Previously Mansour et al.[52] have reported that optical limiting exhibited by carbon black dispersions was almost entirely due to thermally induced nonlinear scattering of the incident laser pulse. Similarly it has been demonstrated recently that optical limiting exhibited by multiwalled carbon nanotube dispersions is almost certainly due to scattering combined with possible electronic absorption contributions.[7−14] In light of this, the nanoparticles that were tested here with dimensions in the region of 50 nm could also exhibit appreciable nonlinear optical extinction due to scattering. This has been recognized above, and thus the parameters discussed for the phthalocyanine nanoparticle dispersions are thought of as coefficients that define only the magnitude and not the nature of the nonlinear optical response. In addition the rise time of the nonlinear optical dissipation was not probed in this study. Miles,[53] in his work

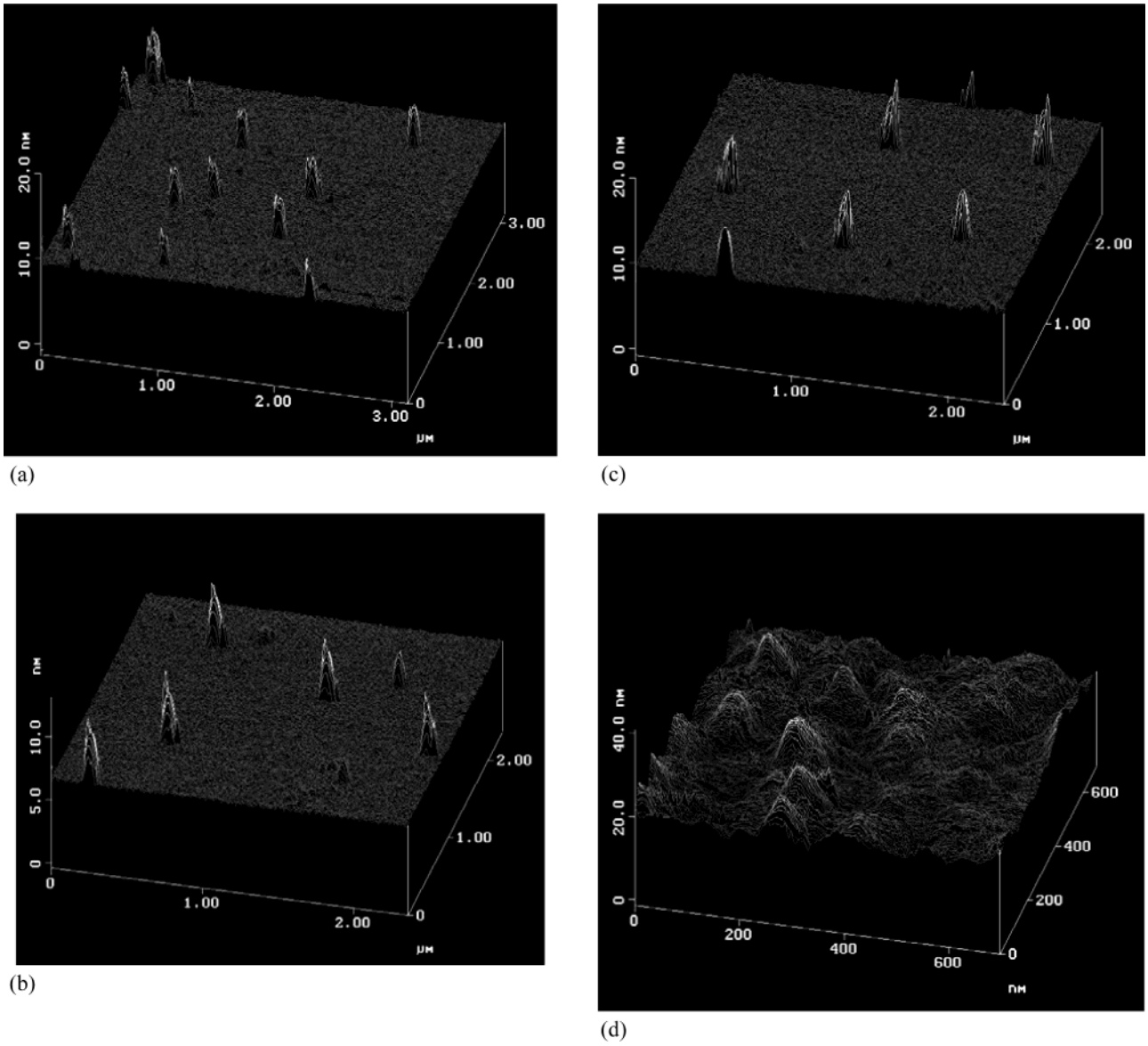

Figure 6. AFM pictures of (a) tBu$_4$PcCu, (b) (PhS)$_4$PcZn, (c) tBu$_4$PcZn, and (d) (PhS)$_4$PcH$_2$.

TABLE 4: Summary of Particle Dimensions[a]

sample	particle size (TEM) [nm]	particle height (AFM) [nm]	low spacing (X-ray) [nm]	high spacing (X-ray) [nm]
tBu$_4$PcZn	51.5	6.74	0.282	0.349
(PhS)$_4$PcZn	67.4	4.01	0.234	0.286
tBu$_4$PcCu	54.6	6.02	0.294	0.356

[a] The particle size is adopted from the results obtained by TEM. The particle heights are taken from the results received in the AFM. The numbers illustrated for the low and high spacing in the particles are calculated from the X-ray diffraction measurements.

concerning the design of practical optical limiters, discussed this point where the leading edge of an optical pulse can damage the protected target before the nonlinearity responds effectively. Phthalocyanines behaving as reverse saturable absorbers have a quick response time in the picosecond regime characteristic of electronic interactions, but nonlinearities associated with scattering generally respond at best in the nanosecond regime. These issues are of immediate concern, and studies are underway to elucidate the temporal behavior of the nanoparticle−optical pulse interaction.

3.2. Particle Structure. In the TEM pictures of tBu$_4$PcCu, (PhS)$_4$PcZn, and tBu$_4$PcZn, it can be seen that the particles are of spherical shape. In all pictures, a clustering effect of the nanoparticles can be seen. Clustering of nanoparticles is a well-known effect and enhanced in this case by the aforementioned sample preparation. With evaporation of the solvent, the spatial separation of the particles is reduced. This decrease of particle separation increases the possibility of collisions between single particles, which causes the effect of clustering. Nevertheless, uniform nanoparticles can be clearly seen as depicted in Figure 5a,b,c. The average sizes are summarized in Table 4. For the (PhS)$_4$PcH$_2$, no uniform nanoparticles were observed. The observed samples showed in general a layer of amorphous material instead of single particles as demonstrated in Figure 5d. Only a few particles of approximately 70 nm in diameter were observed.

The particle diameters determined by TEM were confirmed by AFM. Furthermore, the height of the particles could be observed by using this method. The particle diameter determined by AFM was in good agreement with the results received by TEM. Apart from a small amount of smaller particles, less than

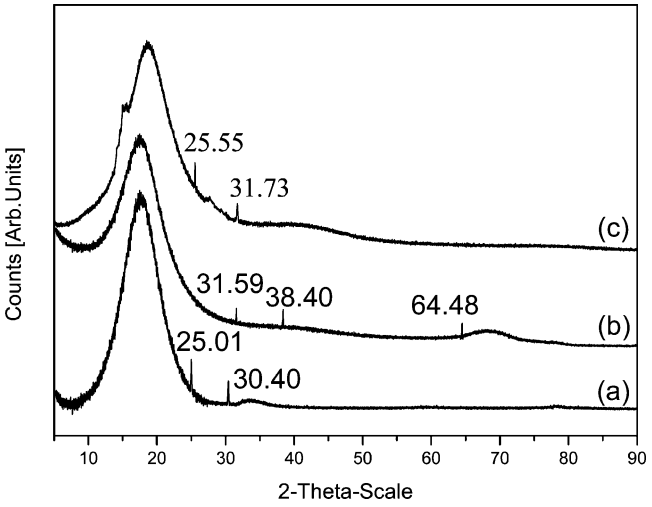

Figure 7. X-ray diffraction patterns of (a) *t*Bu_4PcCu, (b) $(PhS)_4$PcZn, and (c) *t*Bu_4PcZn.

5% on average, all of these images showed similar heights with a variation of approximately 0.2 nm. The determined heights are presented in Table 4. Typical AFM images are depicted in Figure 6. Again, the images of the PcH_2 showed only a few particles of different sizes. Nevertheless, the very noisy surface signal gives rise to various arrangements of molecules on the silicon substrate. This is in good agreement with the results obtained by TEM and the edge-to-edge stacking concluded from the UV/vis spectroscopy.

X-ray diffraction measurements were performed to further investigate the general arrangement of molecules in the particle. In the case of*t*Bu_4PcCu, $(PhS)_4$PcZn, and *t*Bu_4PcZn particles, clear diffraction patterns could be observed as shown in Figure 7. This is indicative of a highly ordered or perhaps even semicrystalline arrangement in these particles. The strong peak at around 19 and the weak peak at around 70−80 on the 2θ-scale are due to the silicon surface and can be neglected. For the $(PhS)_4PcH_2$, no X-ray diffraction spectrum could be obtained. This was not unexpected as the previous results all indicate that there was little or no particle formation with this compound. By using Bragg's law ($n\lambda = 2d \sin \theta$), we can convert the peak positions of the diffraction peaks into distances. The two peaks were assumed to represent the distance to the next molecule stacked edge-to-edge and the distance to the next molecule stacked in a sandwich-type formation, respectively. The peak for $(PhS)_4$PcZn at 64.48 was assumed to be a second-order peak. The results are presented in Table 4.

Taking all aforementioned approximations and results into account, neglecting the possible trapping of solvent in the particle, a simplified nanoparticle structure model as shown in Figure 8 can be considered. It should be noted that the following calculations are highly simplified compared to the actual systems and the resulting numbers should be interpreted with care. They are a simplified interpretation of the particle structure. The volume of this particle can be calculated as

$$V_{\text{particle}} = {}^4/_3(\pi b a^2) \quad (1)$$

where V_{particle} is the particle volume, b represents half of the particle height, and a is half of the diameter. To estimate the area of the particle surface, "Guldinsch Rule" was used. This rule considers the surface area of the particle, A_{particle}, to be

$$A_{\text{particle}} = (LV_{\text{particle}})/F_{\text{p}} \quad (2)$$

where L refers to half of the circumference, given by $(2\pi a)/2$ for the nanoparticle. The volume of the particle is given by V_{particle}, and F_{p} represents the projection of half of the particle area, given by $(\pi a^2)/2$.

The volume for each phthalocyanine molecule can be estimated as

$$V_{\text{molecule}} = LWH \quad (3)$$

where L refers to the length and W the width of the molecule. Both numbers were calculated by using ChemSketch 3.5 in 3D mode. As shown in Figure 9 for $(PhS)_4$PcZn, the length and width of the molecules are approximately equal even when one considers that phthalocyanines generally exist in different isomeric configurations. Furthermore, this length−width value has to be increased by the distance to the next "edge-to-edge" stacked molecule in the particle, termed the "high spacing" in Table 4 determined from the X-ray diffraction measurements. The height, H, of the molecule is given by the distance to the next "sandwich" stacked particle, termed "low spacing" in Table 4 from the X-ray diffraction results. Due to the planar structure of the macrocycle, the height of the molecule calculated in ChemSketch 3.5 was neglected when estimating its surface area. The surface area of the phthalocyanine molecule can therefore be approximated as

$$A_{\text{molecule}} = 2LW \quad (4)$$

where L and W represent the molecule diameters increased by the distance to the next neighbor molecule.

By dividing the particle volume (V_{particle}) by the volume of a single molecule (V_{molecule}), an approximation to the amount of molecules in each particle can be obtained. The number of surface molecules per particle can be estimated by dividing the particle surface area (A_{particle}) by half of the area of a molecular surface (A_{molecule}). These results are summarized in Table 5.

4. Conclusions

This study involved the fabrication and characterization of phthalocyanine nanoparticles. The aim of these investigations was to influence the linear and nonlinear optical properties of

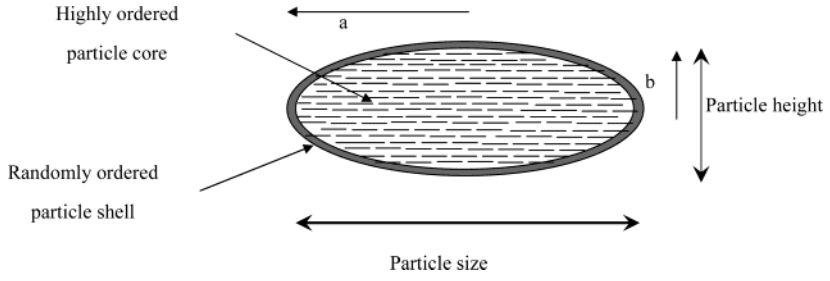

Figure 8. Simplified model of a phthalocyanine nanoparticle.

TABLE 5: Molecule Volume, Surface Area, and Number of Molecules on the Surface

sample	$V_{molecule}$ [nm^3]	molecules per particle (×1000)	length/width molecules [nm]	$A_{molecule}$ [nm^2]	molecules at surface (×1000)	number of surface atoms [%]
*t*Bu$_4$PcZn	0.99	9.5	1.52	7.0	0.2	2.0
(PhS)$_4$PcZn	1.18	8.0	1.96	10.0	0.1	1.5
*t*Bu$_4$PcCu	1.03	9.0	1.52	7.0	0.2	2.0

the phthalocyanines by exploiting intermolecular interactions between single molecules. Furthermore, a general suitable method for controlled aggregation of phthalocyanine was demonstrated. The phase change from solution to quasi-solid-state that was demonstrated could be useful for possible application in optical limiting devices. The particle preparation method chosen was the "microwave method", which is a novel combination of reprecipitation and microwave irradiation. The actual particle size, which was on the nanometer scale, was found to be molecule-dependent. However, it could be seen that this method was not suitable for phthalocyanines without a central metal. Linear optical absorption spectroscopy (UV/vis) was performed on the particles and compared with solutions of the starting compounds. The UV/vis spectra exhibited a quenching of the Q-band absorption peak and a broadening into blue- and red-shifted components for the nanoparticles compared to the molecular solutions. This is expected behavior for aggregated molecules. Furthermore, the B-band absorption increased significantly in particle state compared to molecules in solution. Fluorescence spectra showed that the phthalocyanines in the nanoparticle state did not fluoresce. These results indicated an aggregated structure in the particle where the optical properties were strongly influenced by intermolecular interactions. Optical limiting studies were performed using an open Z-scan set up at 532 nm in the nanosecond regime. The nanoparticles were found to have an increased ratio of the effective excited-state absorption to the ground-state absorption cross section, κ, within a three-level description of the process. This ratio is one of the characteristic numbers in optical limiting studies and has been utilized as an indicator of optical limiting performance. The phase shift from molecular to particle state increases the nonlinear absorption in the phthalocyanine system by approximately a factor of 3.

Transmission electron microscopy (TEM) analysis led to a further understanding of the dimensional structure of these nanoparticles in two dimensions. Under the use of high magnification, they were found to display uniform circular shapes. Atomic force microscopy (AFM) was used to confirm this structure and additionally to determine the actual height of the particles. These microscopy studies revealed that the nanoparticles possessed an oblate ellipsoidal shape. X-ray diffraction measurements were performed to gain more understanding of the molecule alignment inside the particle. The clear appearance of diffraction pattern peaks was observed. This indicated a structure of highly ordered phthalocyanine molecules in the particle.

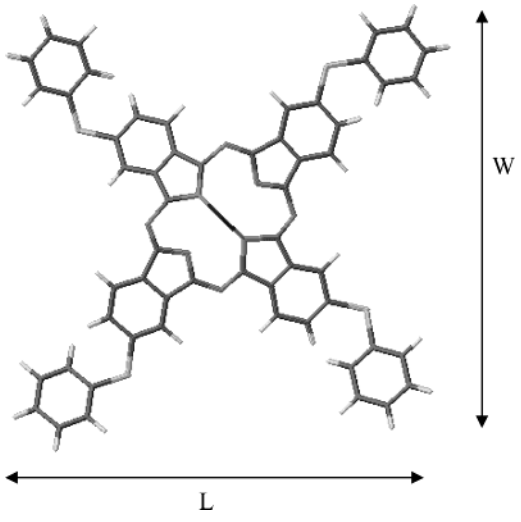

Figure 9. Length and width of a phthalocyanine molecule.

By combining the results, a generalized and simplified model for the nanoparticles was discussed. In this model, the particles consist of a core where the molecules are in a highly ordered alignment and an outer shell in which single molecules are in a random order. The number of molecules per particle was estimated, and furthermore, the ratio of surface molecules to molecules per particle was also estimated. This number was previously found to be an important value in inorganic cluster and colloid systems, which are similar to the system studied here.

Further work can be split into two distinct categories. The first significant and pressing issue in this field is control over the nanoparticle size and consequently the arrangement of constituent molecules in the nanoparticles. For solid-state applications, a very interesting possibility could be the use of polymer as a tool to avoid uncontrolled aggregation of particles. Once "trapped" in a polymer matrix, the linear and nonlinear optical properties of thin films, prepared by that composite, could be investigated.. The second issue to be addressed is the origin of the optical nonlinearity exhibited by the nanoparticle dispersions. Transient absorption studies and pump−probe spectroscopy will reveal the nature of the excited state of the nanoparticles and the effects of scattering contributions to the nonlinear optical dissipation.

Acknowledgment. The authors gratefully acknowledge the support of the Irish Higher Education Authority (HEA), Enterprise Ireland, and the European Union under contract number HPRN-CT-2000-00020. Furthermore, we acknowledge the TCD CMA (Centre for Microscopy and Analysis) and contributions of A. Strevens. C.N. acknowledges the contributions of James Doyle, Dr. Stefanie Maier, and Dr. Manuel Rüther.

References and Notes

(1) Tutt, L. W.; Boggess, T. F. *Prog. Quantum Electron.* **1993**, *17* (4), 299−338.

(2) Bindra, K. S.; Oak, S. M.; Rustagi, K. C. *Opt. Commun.* **1996**, *124* (5−6), 452−456.

(3) Justus, B. L.; Campillo, A. J.; Hendershot, D. G.; Gaskill, D. K. *Opt. Commun.* **1993**, *103* (5−6), 405−409.

(4) Henari, F.; Callaghan, J.; Stiel, H.; Blau, W.; Cardin, D. J. *Chem. Phys. Lett.* **1992**, *199* (1−2), 144−148.

(5) Henari, F.; Cazzini, K.; Weldon, D.; Blau, W. *Appl. Phys. Lett.* **1995**, *68* (5), 619−621.

(6) Izaac Elim, H.; Ouyang, J.; He, J.; Hong Goh, S.; Hai Tang, S.; Ji, W. *Chem. Phys. Lett.* **2003**, *369* (3−4), 281−286.

(7) Vivien, L.; Anglaret, E.; Riehl, D.; Bacou, F.; Journet, C.; Goze, C.; Andrieux, M.; Brunet, M.; Lafonta, F.; Bernier, P.; Hache, F. *Chem. Phys. Lett.* **1999**, *307* (5−6), 317−319.

(8) Vivien, L.; Anglaret, E.; Riehl, D.; Hache, F.; Bacou, F.; Andrieux, M.; Lafonta, F.; Journet, C.; Goze, C.; Brunet, M.; Bernier, P. *Opt. Commun.* **2000**, *174* (1−4), 271−275.

(9) Liu, L.; Zhang, S.; Hu, T.; Guo, Z. X.; Ye, C.; Dai, L.; Zhu, D. *Chem. Phys. Lett.* **2002**, *359* (3−4), 191−195.

(10) Mishra, S. R.; Rawat, H. S.; Mehendale, S. C.; Rustagi, K. C.; Sood, A. K.; Bandyopadhyay, R.; Govindaraj, A.; Rao, C. N. R. *Chem. Phys. Lett.* **2000**, *317* (3−5), 510−514.

(11) Vivien, L.; Lancon, P.; Riehl, D.; Hache, F.; Anglaret, E. *Carbon* **2002**, *40* (10), 1789−1797.

(12) Vivien, L.; Riehl, D.; Hache, F.; Anglaret, E. *Physica B* **2002**, *323* (1−4), 233−234.

(13) O'Flaherty, S. M.; Hold, S. V.; Brennan, M. E.; Cadek, M.; Drury, A.; Coleman, J. N.; Blau, W. J. *J. Opt. Soc. Am. B* **2003**, *20* (1), 49−58.

(14) O'Flaherty, S. M.; Murphy, R.; Hold, S. V.; Cadek, M.; Coleman, J. N.; Blau, W. J. *J. Phys. Chem. B* **2003**, *107*, 958−964.

(15) Idrish Miah, M. *Opt. Mater.* **2002**, *20* (4), 279−282.

(16) Fang, H.; Du, C.; Qu, S.; Li, Y.; Song, Y.; Li, H.; Liu, H.; Zhu, D. *Chem. Phys. Lett.* **2002**, *364* (3−4), 290−296.

(17) Qu, S.; Du, C.; Song, Y.; Wang, Y.; Gao, Y.; Liu, S.; Li, Y.; Zhu, D. *Chem. Phys. Lett.* **2002**, *356* (3−4), 403−408.

(18) Pang, Z.; Zhao, L.; Chen, M. Q.; Wang, J. Y.; Li, Y. F. *Polyhedron* **2002**, *21* (27−28), 2675−2681.

(19) Claessens, C. G.; Blau, W. J.; Cook, M.; Hanack, M.; Nolte, R. J. M.; Torres, T.; Wöhrle, D. *Monatsh. Chem.* **2001**, *132*, 3−11.

(20) Zyss, J. *Nonlinear Optics: Materials, Physics, and Devices*; Academic Press: Boston, MA, 1993.

(21) Chemla, D.; Zyss, J. *Nonlinear optical properties of organic molecules and crystals*; Academic Press: Orlando, FL, 1987; Vol. 2.

(22) Nalwa, H.; Miyata, S. *Nonlinear optics of molecules and polymers*; CRC Press: Boca Raton, FL, 1997.

(23) Nalwa, H. S.; Shirk, J. S. In *Phthalocyanines: Properties and Applications*; Leznoff, C. C., Lever, A. B. P., Eds.; John Wiley & Sons: New York, 1996.

(24) Mckeown, N. B. In *Phthalocyanine Materials: Synthesis, Structure and Function*; Dunn, B., Goodby, J. W., West, A. R., Eds.; Cambridge University Press: Cambridge, U.K., 1998.

(25) Coulter, D. R.; Miskowski, V. M.; Perry, J. W.; Wei, T. H.; Van Stryland, E. W.; Hagan, A. D. J. *SPIE Proc.* **1989**, *1105*, 42.

(26) Shirk, J. S.; Pong, R. G. S.; Flom, S. R.; Heckmann, H.; Hanack, M. *J. Phys. Chem. A* **2000**, *104* (7), 1438−1449.

(27) Shirk, J. S.; Pong, R. G. S.; Bartoli, F. J.; Snow, A. W. *Appl. Phys. Lett.* **1993**, *63* (14), 1880−1882.

(28) Perry, J. W.; Mansour, K.; Lee, I. Y. S.; Wu, X. L.; Bedworth, P. V.; Chen, C. T.; Ng, D.; Marder, S. R.; Miles, P.; Wada, T.; Tian, M.; Sasabe, H. *Science* **1996**, *273*, 1533−1536.

(29) Suchozak, B. *York Chem. Soc. Gazette* **1999**, *1*.

(30) Bosshard, C.; Pan, F.; Wong, M. S.; Manetta, S.; Spreiter, R.; Cai, C.; Gunter, P.; Gramlich, V. *Chem. Phys.* **1999**, *245* (1−3), 377−394.

(31) Desiraju, G. R. *Curr. Opin. Solid State Mater. Sci.* **1997** *2* (4), 451−454.

(32) Oshikiri, T.; Kasai, H.; Katagi, H.; Okada, S.; Oikawa, H.; Nakanishi, H. *Mol. Cryst. Liq. Cryst. Sci. Technol., Sect. A* **1999**, *337*, 25−30.

(33) Baba, K.; Kasai, H.; Okada, S.; Oikawa, H.; Nakanishi, H. *Jpn. J. Appl. Phys., Part 2* **2000**, *39* (12A), L1256−L1258.

(34) Sarkar, A.; Okada, S.; Matsuzawa, H.; Matsuda, H.; Nakanishi, H. *J. Mater. Chem.* **2000**, *10*, 819−828.

(35) Oikawa, H.; Oshikiri, T.; Kasai, H.; Okada, S.; Tripathy, S. K.; Nakanishi, H. *Polym. Adv. Technol.* **2000**, *11* (8−12), 783−790.

(36) Nitschke, C.; O'Flaherty, S.; Kroell, M.; Blau, W. *Chem. Phys. Lett.*, in press.

(37) Jun, Y.-W.; Jung, Y.-Y.; Cheon, J. *J. Am. Chem. Soc.* **2002**, *124* (4), 615−619.

(38) Komai, Y.; Kasai, H.; Hirakoso, H.; Hakuta, Y.; Katagi, H.; Okada, S.; Oikawa, H.; Adschiri, T.; Inomata, H.; Arai, K.; Nakanishi, H. *Jpn. J. Appl. Phys., Part 2* **1999**, *38* (1AB), L81−L83.

(39) Hong-Zheng Chen, C.; Wang, M. *NanoStruct. Mater.* **1999**, *11* (4), 523−520.

(40) Yamamoto, T.; Wada, Y.; Yin, H. B.; Sakata, T.; Mori, H.; Yanagida, S. *Chem. Lett.* **2002**, No. 10, 964−965.

(41) Wada, Y.; Kuramoto, H.; Anand, J.; Kitamura, T.; Sakata, T.; Mori, H.; Yanagida, S. *J. Mater. Chemi.* **2001**, *11* (7), 1936−1940.

(42) Wada, Y.; Kuramoto, H.; Sakata, T.; Mori, H.; Sumida, T.; Kitamura, T.; Yanagida, S. *Chem. Lett.* **1999**, No. 7, 607−608.

(43) Sheik-Bahae, M.; Said, A. A.; Wei, T.-H.; Hagan, D. J.; Van Stryland, E. W. *J. Quantum Electron.* **1990**, *26*, 760.

(44) Wrobel, D.; Boguta, A. *J. Photochem. Photobiol., A* **2002**, *150* (1−3), 67−76.

(45) Endo, K.; Kondo, Y.; Aoyama, Y.; Hamada, F. *Tetrahedron Lett.* **2003**, *44* (7), 1355−1358.

(46) Balaban, T. S.; Eichhöfer, A.; Lehn, J.-M. *Eur. J. Org. Chem.* **2000**, 4047−4057.

(47) Kasha, M.; Rawls, H. R.; El-Bayoumi, M. A. *Pure Appl. Chem.* **1965**, *11*, 371.

(48) Antonov, L.; Gergov, G.; Petrov, V.; Kubista, M.; Nygren, J. *Talanta* **1999**, *49*, 99−106.

(49) Ogawa, K.; Kobuke, Y. *Angew. Chem., Int. Ed.* **2000**, *39* (22), 4070−4073.

(50) Czikklely, V.; Forsterling, H. D.; Kuhn, H. *Chem. Phys. Lett.* **1970**, *6* (3), 207−210.

(51) Chen, Y.; O'Flaherty, S.; Fujitsuka, M.; Hanack, M.; Subramanian, L. R.; Ito, O.; Blau, W. J. *Chem. Mater.* **2002**, *14*, 5163−5168.

(52) Mansour, K.; Soileau, M. J.; Van Stryland, E. W. *J. Opt. Soc. Am. B* **1992**, *9*, 1100−1109.

(53) Miles, P. A. *Appl. Opt.* **1994**, *33*, 6965−6979.